THE JOURNAL OF BIOLOGICAL CHEMISTRY VOL. 290, NO. 45, pp. 27215–27227, November 6, 2015

Correlations between Photodegradation of Bisretinoid Constituents of Retina and Dicarbonyl Adduct Deposition*

Received for publication, August 2, 2015, and in revised form, September 15, 2015 Published, JBC Papers in Press, September 22, 2015, DOI 10.1074/jbc.M115.680363

Jilin Zhou[‡], **Keiko Ueda**[‡], **Jin Zhao**[‡], **and Janet R. Sparrow**[‡§1]

From the Departments of [‡]*Ophthalmology and* [§]*Pathology and Cell Biology, Columbia University Medical Center, New York, New York 10032*

Background: The origin of adduct-forming and cross-linking species in aging Bruch's membrane of the eye is unclear.
Results: Mechanistic studies indicate links between photodegradation of bisretinoids of retinal pigment epithelial (RPE) cells and dicarbonyl adduct deposition.
Conclusion: Dicarbonyl release from overlying RPE may be a factor in Bruch's membrane deposition.
Significance: These processes could contribute to age-related macular degeneration.

Non-enzymatic collagen cross-linking and carbonyl adduct deposition are features of Bruch's membrane aging in the eye, and disturbances in extracellular matrix turnover are considered to contribute to Bruch's membrane thickening. Because bisretinoid constituents of the lipofuscin of retinal pigment epithelial (RPE) cells are known to photodegrade to mixtures of aldehyde-bearing fragments and small dicarbonyls (glyoxal (GO) and methylglyoxal (MG)), we investigated RPE lipofuscin as a source of the reactive species that covalently modify protein side chains. *Abca4*$^{-/-}$ and *Rdh8*$^{-/-}$/*Abca4*$^{-/-}$ mice that are models of accelerated bisretinoid formation were studied and pre-exposure of mice to 430 nm light enriched for dicarbonyl release by bisretinoid photodegradation. MG protein adducts were elevated in posterior eyecups of mutant mice, whereas carbonylation of an RPE-specific protein was observed in *Abca4*$^{-/-}$ but not in wild-type mice under the same conditions. Immunolabeling of cryostat-sectioned eyes harvested from *Abca4*$^{-/-}$ mice revealed that carbonyl adduct deposition in Bruch's membrane was accentuated. Cell-based assays corroborated these findings in mice. Moreover, the receptor for advanced glycation end products that recognizes MG and GO adducts and glyoxylase 1 that metabolizes MG and GO were up-regulated in *Abca4*$^{-/-}$ mice. Additionally, in acellular assays, peptides were cross-linked in the presence of A2E (adduct of two vitamin A aldehyde and ethanolamine) photodegradation products, and in a zymography assay, reaction of collagen IV with products of A2E photodegradation resulted in reduced cleavage by the matrix metalloproteinases MMP2 and MMP9. In conclusion, these mechanistic studies demonstrate a link between the photodegradation of RPE bisretinoid fluorophores and aging changes in underlying Bruch's membrane that can confer risk of age-related macular degeneration.

The dicarbonyl molecules methylglyoxal (MG)[2] and glyoxal (GO) are highly reactive clinically relevant molecules that are implicated in the molecular damage that accompanies aging changes (1) and chronic disease states such as diabetes and uremia (2). In diabetes, MG and GO are best known for being major precursors of carbonyl adducts (advanced glycation end products, AGEs) that form non-enzymatically from the degradation of sugar-phosphate intermediates such as glyceraldehyde 3-phosphate and dihydroxyacetone phosphate (3). Chronic hyperglycemia in diabetes accelerates the formation of these dicarbonyl adducts, and the resulting protein modifications are strongly correlated with the development and progression of diabetic vascular disease and its complications (4).

The adverse effects of MG and GO on cellular function follow the nonenzymatic reactions of dicarbonyls with the thiol and free amino groups of proteins, nucleotides, and basic phospholipids (5). Preferential modification of arginine residues occurs by irreversible reaction with MG (MG-derived hydroimidazolone adducts, MG-H1) and is particularly problematic as this amino acid is frequently located at functional sites of proteins (2). Less abundant are the adducts formed by MG and GO with lysine (carboxyethyl-lysine and carboxymethyl-lysine, respectively). Because these highly reactive dicarbonyls are bifunctional molecules carrying two aldehydes (GO) or an aldehyde and a ketone (MG), they can also form cross-linked species such as methylglyoxal-derived lysine dimer and glyoxal-derived lysine dimer. Arg pyrimidine, an adduct of MG and arginine, has intrinsic fluorescence (385 nm emission) (6).

We have demonstrated that a previously unknown source of MG and GO is the photooxidation-induced photodegradation of the vitamin A aldehyde-derived molecules, including A2E (adduct of two vitamin A aldehyde and ethanolamine) and all-*trans*-retinal dimer, that accumulate in retinal pigment epithelial (RPE) cells as bisretinoid constituents of RPE lipofuscin (7,

* This work was supported by National Institutes of Health Grants EY12951 and P30EY019007, Foundation Fighting Blindness, and a grant from Research to Prevent Blindness (to the Dept. of Ophthalmology, Columbia University). The authors declare that they have no conflicts of interest with the contents of this article.
[1] To whom correspondence should be addressed: Dept. of Ophthalmology, Columbia University, 635 W. 165th St., New York, NY 10032. Tel.: 212-305-9944; E-mail: jrs88@columbia.edu.

[2] The abbreviations used are: MG, methylglyoxal; GO, glyoxal; RPE, retinal pigment epithelial; RAGE, receptor for advanced glycation end product; AGE, advanced glycation end; ANOVA, analysis of variance; DNPH, dinitrophenylhydrazine; DNP, 2,4-dinitrophenol hydrazine; MG-H1, MG-derived hydroimidazolone; MMP, matrix metalloproteinase; hMMP, human MMP; AMD, age-related macular degeneration; MG-H1, MG-derived hydroimidazolone; qPCR, quantitative PCR.

8). By employing liquid chromatography coupled to electrospray ionization mass spectrometry together with tandem mass spectrometry (MS/MS), we identified MG and GO along with other aldehyde-bearing fragments within the photo-fragments released by the irradiation of the bisretinoids A2E and all-*trans*-retinal dimer. We trapped MG by derivatization with 4-nitrophenylhydrazine, and we showed that bisretinoid photo-cleavage would occur at sites of singlet molecular oxygen addition within the polyenic structures of the bisretinoid molecules A2E and all-*trans*-retinal dimer (7, 8). We also demonstrated that these photofragments can be released from cultured cells into the extracellular milieu.

Although the generation of MG and GO by photodegradation of lipofuscin may not be relevant to diabetes, it could be important for understanding the disease processes in various forms of macular degeneration. The pathogenesis of age-related macular degeneration (AMD) is thought to begin with the RPE and subjacent Bruch's membrane. Bruch's membrane undergoes age-related changes especially in the sub-macular region; these changes include increased thickness (9), lipid accumulation (10), non-enzymatic collagen cross-linking (11, 12), and formation of focal deposits (drusen) (13). Proteins in Bruch's membrane and drusen have been shown to carry modifications in the form of carbonyl adducts of the AGE class (14, 15). Bruch's membrane is prone to AGE accumulation because the resident proteins are particularly long-lived (16). This dicarbonyl accumulation induces an aging mRNA phenotype (17), up-regulates receptors for AGE (RAGE) in overlying RPE (14, 18, 19), promotes lipid retention in Bruch's membrane (20), and reduces RPE adhesion (21). Ligand binding to RAGE incites or amplifies inflammatory processes (22). RAGE also serves as a receptor for other components of drusen, including β-amyloid (23). In this work, we have utilized mouse and *in vitro* models to explore the contribution made by RPE lipofuscin to dicarbonyl adduct deposition. The mouse models include $Abca4^{-/-}$ mice; these mutant mice undergo accelerated bisretinoid lipofuscin accumulation and photoreceptor cell degeneration (24–26).

Experimental Procedures

Mouse Models—Albino *Abca4/Abcr* null mutant mice ($Abca4^{-/-}$) (27), pigmented $Rdh8^{-/-}/Abca4^{-/-}$ mice (gift from Dr. Krzysztof Palczewski, Case Western Reserve University), pigmented $Rpe65^{rd12}$ mice (The Jackson Laboratory, Bar Harbor, ME), and albino $Abca4^{+/+}$ mice, all of which were homozygous for Rpe65-Leu-450, were housed under a 12-h on-off cyclic lighting with in-cage illuminance of ~40 lux. Genotyping for the rd8 mutation in Crb1 was performed using previously described primers and protocol (28). The $Abca4^{-/-}$ mice did not carry the rd8 mutation, although the $Rdh8^{-/-}/Abca4^{-/-}$ mice were homozygous for the mutation. Because wavelengths in the blue region of the spectrum excite a mixture of lipofuscin fluorophores (29), in some experiments, mice were exposed in-cage to 430 nm light from a halogen source (1 milliwatt; measured with Newport Optical Power Meter Model 840; Irvine, CA) for 2 h each day for 7 days before euthanasia. The research was approved by the Institutional Animal Care and Use Committee (IACUC) and was performed in accordance with the ARVO Statement for the Use of Animals in Ophthalmic and Visual Research.

Synthesis—A2E and all-*trans*-retinal dimer were synthesized using starting materials and conditions as described previously; purification was by HPLC (30, 31).

Cell Culture—Human adult RPE (ARPE-19, American Type Culture Collection, Manassas, VA) deficient in endogenous lipofuscin (32) were grown to confluence as described previously (33). For some experiments, the cells were plated on culture surfaces coated with human type IV collagen (Sigma) by incubating at 40 μg/cm^2 for 3 h at room temperature. Where indicated, synthesized A2E was introduced to the cultures (10 μM) for accumulation in the lysosomal compartment of the cells (32). Freshly prepared A2E in the culture medium was delivered twice a week, and accumulation proceeded for 2 weeks. The cells were exposed to 430 nm of irradiation (1.5 milliwatts/cm^2, 20 min) to photooxidize A2E (34, 35), and the cells were subsequently incubated for 6 h.

Detection of Protein Carbonylation by Western Blotting—For immunoblot detection of *in vivo* carbonylation of Rpe65, the dinitrophenylhydrazine (DNPH)-based method was used (36, 37). Dissected posterior eyecups of mice (eight eyes/sample) were placed in lysis buffer (Tris-HCl, pH 7.5, Cell Signaling Technology Inc., Danvers, MA) with 150 mM sodium chloride, detergent (Nonidet P-40, 0.5% sodium deoxycholate), 0.7 μg/ml pepstatin, and a protease inhibitor mixture (Roche Applied Science). The samples were homogenized on ice by sonication for 10–15 s. After centrifugation (14,000 rpm at 4 °C), the protein concentration in the supernatant was determined, and Rpe65 was immunoprecipitated with rabbit monoclonal anti-Rpe65 antibody (Abcam; ab175936) and protein A/G-coupled agarose beads (Roche Applied Science). The immunoprecipitated samples were boiled and separated on 10% Mini-Protean TGX gels (Bio-Rad) together with molecular weight standards (Cell Signaling Technology). The proteins were then transferred to an activated polyvinylidene fluoride (PVDF) membrane (Bio-Rad), and after equilibrating the membrane in methanol, the membrane was incubated in 1 mM DNPH in 2 N HCl (5 min) to derivatize carbonyls. Subsequently, carbonyl adducts were detected by immunoreactivity with rabbit anti-DNP (Cell Biolabs; catalog no. 230801) and HRP-conjugated secondary antibody (Cell Biolabs) with enhanced chemiluminescence (ECL) development. After the membrane was stripped, it was re-probed with mouse monoclonal anti-RPE65 antibody (Abcam; ab13826).

To analyze the protein carbonyl content in lysates of cultured cells, preboiled protein samples (15 μg of total protein/lane) were subjected to SDS-PAGE for protein separation, transferred to PVDF membranes, derivatized with DNPH, and probed with antibody to DNP as described above. Antigen-antibody complexes were visualized by the ECL reagent and exposure to x-ray films. Carbonylated BSA served as a positive control. After the membrane was stripped, it was re-probed with a monoclonal antibody to β-actin (Abcam; ab6276), with the latter serving as internal (loading) standard. Total lane densities (protein carbonyl) and the densities of the actin bands were determined using ImageJ (National Institutes of Health, Bethesda), and the ratio of protein carbonyl/actin was calcu-

lated. Values were normalized to untreated controls (100%) and plotted.

Detection of MG Adducts and Protein Carbonylation by Enzyme-linked Immunosorbent Assay (ELISA)—For analysis in mice (eight eyes per sample), posterior eyecups were placed in lysis buffer (Cell Signaling, Danvers, MA) with protease inhibitors (complete protease inhibitor mixture tablets, Roche Applied Science), and the samples were sonicated for 10–15 s on ice to shear DNA and reduce sample viscosity. After centrifuging the lysates at 14,000 rpm and 4 °C, the protein concentration of the supernatant was determined using the BCA protein assay (Pierce), and methylglyoxal-derived hydroimidazolone (MG-H1) protein adducts were quantified by competitive indirect ELISA using an HRP-conjugated secondary antibody (OxiSelect, Cell Biolabs). Absorbance was read at 450 nm, and MG content was determined by comparison with a standard curve constructed using MG-BSA, a four-parameter fit algorithm, and absorbance (y) as a function of log concentration (x) (38). To control for the metabolic source of MG, levels of MG-H1 adducts in *Rpe65*^{rd12} mice that do not accumulate lipofuscin (39) were subtracted as background.

MG-H1 protein adducts were also quantified in ARPE-19 cells that had accumulated A2E and were exposed to 430 nm light. Lysates were prepared as described above, and MG-BSA equivalent concentration was determined using the protocol for competitive indirect ELISA as stated.

ARPE-19 cells that had accumulated A2E and were exposed to 430 nm light were also examined in duplicate for protein carbonylation using direct ELISA (OxiSelect, Cell Biolabs). Briefly, after pelleting, the cells were placed in ice-cold PBS and lysed by sonication; the samples were digested with RNase A and DNase I (Sigma), and proteins were precipitated with ammonium sulfate. Protein concentration was determined, and 1 μg of protein was added to each well in a 96-well protein-binding plate and incubated at 4 °C overnight. After derivatizing with DNPH (0.04 mg/ml), protein-bound DNP was detected immunochemically using anti-DNP antibody (OxiSelect, Cell Biolabs, catalog no. 231002) and horseradish peroxidase-conjugated secondary antibody. Absorbance (450 nm) was read in a SpectraMax 5 microplate reader (Sunnyvale, CA). Protein carbonyl content was determined by comparison with the linear range of a standard curve constructed using carbonyl-BSA.

Immunohistochemistry—Mouse eyes were fixed in 2% paraformaldehyde for 40 min, embedded in Tissue-Tek O.C.T compound (Thermo Fisher Scientific, Waltham MA), snap-frozen in liquid nitrogen, and sectioned at 5 μm in a cryostat. All sections were post-fixed with 4% paraformaldehyde for 20 min, air-dried, and sealed in −70 °C for storage. Endogenous peroxidase activity was inhibited with 4.5% H_2O_2 in methanol for 1.5 h at room temperature and then rinsed with PBS. Sections were incubated with 0.2% DNPH (Cell Biolabs) in 2 N HCl for 60 min at room temperature in the dark and then were extensively washed with PBS. To inhibit nonspecific binding, the sections were incubated in 10% goat serum, 0.2% saponin in PBS for 30 min, and then the specimen was incubated for 2 h in rabbit anti-DNP antibodies (1:100; Life Technologies, Inc.; catalog no. A6430) at room temperature. After washing, the sections were incubated with a peroxidase-conjugated goat anti-rabbit Ig (1:500, Jackson ImmunoResearch, West Grove PA; catalog no. 111-035-144) for 1 h, and finally incubated with ImPACT™ AMEC Red Substrate (Vector Laboratories, Burlingame CA) for 15 min. Sections were counterstained with Ehrlich's hematoxylin for 5 min and then mounted in 50% glycerol/PBS. Anti-DNP antibody or the DNPH treatment was omitted for controls. For the detection of MG adducts, sections were blocked and then reacted with rabbit polyclonal antibody raised against MG-keyhole limpet hemocyanin (1:100; Biorbyt, Cambridge UK; orb27266). Primary antibodies were omitted in controls. Sections were imaged with a Leica DM5000B microscope (Leica N PLAN ×63 lens) and a SPOT Pursuit USB 1.4Mp Slider camera (model 34.4) equipped with acquisition software (SPOT advanced imaging software). Images were compiled in Adobe Photoshop CS4 extended (Adobe Systems, San Jose, CA), and the levels command was used to adjust the contrast of all images simultaneously.

Detection of MG-modified Protein by Dot-blot—Human collagen type IV (Sigma) (1 mg/ml) and bovine serum albumin (BSA) (10 mg/ml; Sigma) that were exposed or not exposed to A2E (200 μM in DMSO/PBS), photo-oxidized A2E (200 μM, 1.6 milliwatts/cm^2, 20 min), or MG (Sigma) (5 days, 37 °C) in duplicate was immobilized on nitrocellulose membrane (Bio-Rad). Rabbit polyclonal anti-MG-keyhole limpet hemocyanin antibody (Biorbyt; orb27266) or mouse monoclonal anti-MG (Cell Biolabs; STA-011) was applied followed by HRP-labeled secondary antibody (Vector Laboratories) and ECL (Bio-Rad) development. Commercial MG-BSA (Cell Biolabs) was used as a positive control.

Immunoblotting of Collagen Substrate—Before harvesting the collagen substrate, the cells were washed with DPBS (Life Technologies, Inc.), exposed to 0.5% trypsin/EDTA (Life Technologies, Inc.) for 90 s, and then maintained at −80 °C for 30 min. The cells were then gently removed with DPBS. The collagen was removed from the dish using activated matrix metalloproteinase-9 (MMP-9) (1 μg/ml final concentration; Sigma) in 1 ml of activation buffer (50 mM Tris-HCl, 10 mM calcium chloride, 150 mM sodium chloride, and 0.05% Brij® L23) overnight at 37 °C. After collection, the samples were centrifuged (3 min, 800 rpm), and the supernatant was dried under argon. The samples were boiled for 3 min and subjected to 7.5% SDS-PAGE separation, and after the proteins were transferred to a nitrocellulose membrane (Bio-Rad), the latter was blocked with 5% nonfat dry milk for 2 h at room temperature and incubated with a rabbit polyclonal antibody raised against MG-keyhole limpet hemocyanin adduct (Biorbyt; orb27266) (1:1000 dilution, overnight at 4 °C). Three consecutive washes in PBS containing 0.1% Tween (10 min/wash) were performed, and the membrane was incubated with a biotinylated anti-rabbit secondary antibody followed by avidin conjugated to horseradish peroxidase (HRP) (Vector Laboratories) for 1 h at room temperature. The nitrocellulose membrane was washed, reacted with ECL (Bio-Rad), dried with a Whatman sheet, and exposed to x-ray film.

SDS-PAGE Analysis of Cross-linked Peptide Substrates—A2E (200 μM) together with RNase A (10 mg/ml; Sigma), the peptide somatostatin (10 mg/ml; Sigma), or *N*-acetyl renin substrate tetradecapeptide (10 mg/ml; Sigma) were irradiated (430 nm ±

30 nm; 1.6 milliwatts/cm^2, 20 min) with and without the dicarbonyl scavenger aminoguanidine-HCl (130 mM; Cayman Chemical Co., Ann Arbor, MI). After irradiation, all the samples were incubated at 37 °C for 5 days with constant stirring. The negative controls were peptides in the absence of irradiated A2E, and positive controls included peptide with 260 mM GO and MG (260 mM; Sigma). RNase A and the oligo-peptide samples were analyzed on 8–16% Tris-glycine SDS-polyacrylamide gradient gels (Bio-Rad) (40, 41). Bio-safe molecular weight markers (Bio-Rad) were utilized, and electrophoresis was performed at 150 V for 1.5–2 h.

RNase Activity Assay—A2E (200 μM in PBS with 1% DMSO) was irradiated (1.6 milliwatts/cm^2, 20 min) and combined with 0.01 unit/ml RNase A (50:50 ratio) and incubated at 37 °C for 1 and 3 days. RNase activity was measured by fluorescent assay (RNase Alert QC System, Life Technologies, Inc.) in 96-well plates (black plate/clear bottom) employing a SpectraMax M5 microplate reader (excitation/emission of 490/520 nm). No RNase control (nuclease-free water) was subtracted as background. MG (260 mM) served as positive control.

Matrix Metalloproteinase-2 (MMP-2) Digestion of Fluorescence-labeled Collagen—Fluorescein isothiocyanate-labeled collagen II (1 mg/ml) (EnzChek, Molecular Probes, Life Technologies, Inc.) was incubated with A2E (200 μM), and the mixture was irradiated (1.6 milliwatts/cm^2 for 20 min). Subsequently human recombinant MMP-2 (0.01 μg/200 μl/well and 0.1 μg/200 μl/well; Sigma) activated by 4-aminophenylmercuric acetate (Sigma) was added and incubated for 1 h at room temperature. Fluorescence was read at 490 excitation/520 emission with SpectraMax M5 (Molecular Device Inc. Sunnyvale, CA).

Collagen Zymography—A 10% SDS-polyacrylamide gel modified by addition of 1 mg/ml human collagen IV (Sigma) as proteolytic substrate was subjected to electrophoresis with human MMP-2 or human MMP-9 (50 ng/5 μl; Sigma) mixed with loading buffer under non-reducing conditions. The collagen was preincubated (5 days, 37 °C) with A2E (200 μM), photooxidized A2E (200 μM A2E, 430 nm exposure, 30 min), or with MG (260 mM, Sigma) as positive control. After electrophoresis (90 V, at 4 °C) the gel was renatured in buffer containing 2.5% Triton X-100 for 30 min at room temperature to allow the proteins to regain the tertiary structure necessary for enzymatic activity. Subsequently, the gel was incubated (37 °C, 18 h) in the developing buffer (50 mM Tris-HCl, 5 mM $CaCl_2$, 200 mM NaCl at pH 7.5) containing *p*-aminophenylmercuric acetate (APMA) (1 mM; Sigma) to convert the non-proteolytic pro-MMPs into active MMPs and to allow for enzyme digestion. The collagen in the gel was then stained with Coomassie Blue R-250 (0.5% with 40% methanol and 10% acetic acid) for 2 h at room temperature and destained in methanol and acetic acid until the lysis bands were clear. The collagen-containing gels were scanned at 300 dpi resolution. As a measure of MMP digestion, the optical density of the Coomassie Blue-stained gels at bands corresponding to the apparent molecular masses of MMP-2 (~69 kDa) and MMP-9 (~93 kDa) were quantified by densitometric analysis using ImageJ software. Gray levels in MMP-free (same size rectangular areas) loading lanes were also determined. Bands in the gel having reduced stain reflected MMP enzyme activity and had increased grayscale values. Gray level (GL) intensities in the MMP lysis bands were normalized to the levels in the MMP-free lanes ($GL_{MMP\ band} \div GL_{MMP\text{-}free}$). After normalization $GL_{MMP\text{-}free}$ equals 1), MMP-2/MMP-9 inhibitor II (Santa Cruz Biotechnology, Dallas TX) also served as positive control.

Hydroxyproline Assay—The colorless bands marking the lysis areas of the zymographs were also analyzed for hydroxyproline content. Bands were cut from the gel and hydrolyzed by incubation with HCl acid (12 N, 3 h, 120 °C) in a pressure-tight Teflon-capped vial (United Laboratory Plastics, St. Louis, MO). Equivalent zones outside the lysis area were subtracted as background. The levels of hydroxyproline were measured by a colorimetric assay based on the reaction of oxidized hydroxyproline with 4-(dimethylamino)benzaldehyde (BioVision, Milpitas, CA). Absorbance at 560 nm was measured by spectrophotometry.

Ultraperformance Liquid Chromatography-Mass Spectrometry (UPLC-MS) Analysis of Glyoxal and Methylglyoxal Derivatized with 2,4-Dinitrophenylhydrazones—A2E (200 μM in distilled water with 1% DMSO) was irradiated (430 ± 20 nm, 1.6 milliwatts/cm^2, 20 min) and then incubated with DNPH (2.5 mM) at 37 °C for 10 min. The standards, GO and MG (200 μM in distilled water), were also incubated with DNPH. The derivatized samples were extracted twice by the addition of 10 ml of pentane agitated for 3 min and centrifuged at 4000 rpm for 1 min. The dried samples were subsequently dissolved in 100 μl of water and analyzed by UPLC (5-μl injection volume) (Waters Acquity UPLC system) operating with a Waters Acquity Single Quadrupole mass spectrometer, photodiode array detection at 355 nm, and an Acquity UPLC BEH C18 column (1.7 μm, 2.1 × 50 μm inner diameter). Chromatographic separation was performed using a gradient of acetonitrile in water (0–15 min and 30–100% acetonitrile) and a flow rate of 0.5 ml/min. UPLC-MS was performed with negative ionization and voltages as follows: capillary voltage, 3.0 V; cone voltage, 45 V; extractor voltage, 2 V; and radio frequence lens voltage, 0.1 V. The desolvation gas flow was 800 liters/h; the source temperature was 150 °C, and desolvation temperature was 500 °C.

Real Time Quantitative Polymerase Chain Reaction (RT-qPCR)—Total RNA isolated from the cells and posterior eyecups of mice (eight eyes/sample) was extracted using the RNeasy mini kit (Qiagen, Valencia, CA). cDNA was synthesized with TaqMan reverse transcription reagents kit (Applied Biosystems, Life Technologies, Inc.) using primers for RAGE (RAGE; TaqMan Assay ID Hs00542584_g1), mouse RAGE (Assay ID Mm01134790_g1), mouse glyoxylase 1 (Mm00844954_s1), mouse glyoxylase 2 (Mm00600347_m1), and 18S (internal control) (Assay ID Hs99999901_s1) purchased from Applied Biosystems. The TaqMan MGB probes carried a 6-carboxyfluorescein reporter dye at the 5′ end and a nonfluorescent quencher at the 3′ end. RT-qPCR was performed in s 10-μl reaction volume with 5 μl of 2× TaqMan Master Mix II (Applied Biosystems, Carlsbad, CA), 0.5 μl of 5 μM stock primer/probe, and 10 ng of cDNA. RT-qPCR was performed on an ABI Prism 7900 sequence detection system (Applied Biosystems) with ABI SDS 2.0 software (Applied Biosystems, Life Technologies, Inc.) and triplicate samples. Data are based on two or three experiments. Results were analyzed using

RQ manager 1.2.1 software and utilized the ΔCt (ΔCt; experimental *Ct* minus 18S rRNA *Ct*) and calibrator $\Delta\Delta Ct$ ($\Delta\Delta Ct$; sample ΔCt minus calibrator ΔCt) method for quantification of relative mRNA expression level (42). Results are reported as fold change ($2-\Delta\Delta C_t$) relative to calibrator.

Statistical Analysis—Statistical analysis was carried out using GraphPad Prism, version 6 (GraphPad Software, Inc. La Jolla, CA), and $p < 0.05$ was considered significant.

Results

Carbonyl Modification of Rpe65 in Abca4 Null Mutant Mice—One of the hallmarks of carbonyl moieties (aldehydes and ketones) is their reactivity with protein side chains. Because the photodegradation of bisretinoid is associated with the release of aldehyde-bearing fragments and the reactive dicarbonyl species, MG and GO, we probed for evidence of carbonyl adduct formation in $Abca4^{-/-}$ mutant mice. This mutant mouse served as a model of increased RPE lipofuscin (27, 43, 44). Rather than observing the total carbonyl content in mouse posterior eyecups, we immunoprecipitated Rpe65, a visual cycle protein that is specific to RPE cells. After derivatizing the carbonyl groups in the immunoprecipitate with DNPH, the stable reaction product DNP (45) was detected by immunoblotting with specific antibody to DNP. To test for a link between light-mediated processes and carbonylation of Rpe65 protein, we also pre-exposed the mice to blue light for 2 h each day for a week. As shown in Fig. 1*A*, a carbonylated protein band at 65 kDa also reacted when re-probed with anti-Rpe65 antibody. Carbonyl adducted Rpe65 was not detected in $Abca4^{+/+}$ mice under the same conditions nor in $Rpe65^{rd12}$ cells that do not express Rpe65 (46) and do not accumulate bisretinoid lipofuscin (39, 47).

Carbonylation of A2E-containing ARPE-19 Cells—To further demonstrate a link between bisretinoid photodegradation and protein carbonyl adduct formation, we used a cell culture model within which A2E is allowed to accumulate in the lysosomal compartment of ARPE-19 cells (32). The latter cell line is preferred for these experiments because in primary cultures of RPE, bisretinoids levels are variable due to progressive cell replication and consequent dilution of RPE lipofuscin. We irradiated A2E-containing ARPE-19 cells, and after collecting cell lysates, we tagged carbonyls by derivatization with DNPH. We used this approach to analyze by both ELISA and Western blot. By SDS-PAGE followed by Western blotting with the antibody that specifically recognizes the stable reaction product DNP conjugated to protein (45), an increase in total protein carbonyl levels in samples of 430 nm exposed A2E-RPE-19 cells was confirmed (Fig. 1*B, panel i*). Multiple protein carbonyl bands in the gradient gels were observed, and individual bands were largely unresolved. Densitometric quantification of the total carbonyl content with values expressed as carbonyl protein/actin ratios revealed a 2-fold increase in the irradiated A2E-containing cells (Fig. 1*B, panel ii*). Protein carbonyls did not reach detectable levels in control ARPE-19 cells or unirradiated A2E-containing ARPE-19 cells when these samples were processed under the same conditions.

Fig. 1*C* illustrates the detection and quantitation of carbonyl-modified protein by ELISA. The carbonyl content in ARPE-19 cells that had accumulated A2E was not different from background. However, when the cells were irradiated at 430 nm, a 4-fold increase was observed after a 2-h incubation, and a more than 60-fold increase was recorded after 6 h. The increase in carbonyl content could be due to the oxidation of various amino acid residues but perhaps predominantly arginine (2).

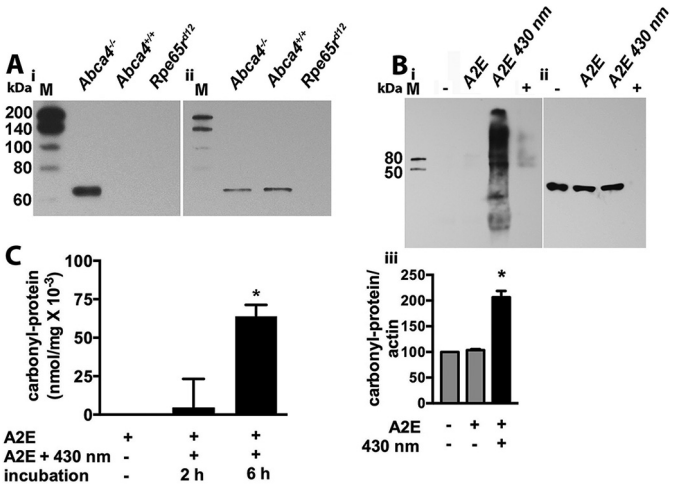

FIGURE 1. **Detection of carbonyl-modified protein.** *A*, carbonylation of Rpe65 in $Abca4^{-/-}$ mice. Rpe65 was immunoprecipitated from posterior eyecups of mice. Samples were subjected to SDS-PAGE, derivatized with DNPH, probed with antibody to DNP (*panel i*), and re-probed with antibody to Rpe65 (*panel ii*). *M* indicates molecular weight markers. $Abca4^{-/-}$, 7 months; $Abca4^{+/+}$, 12 months; $Rpe65^{rd12}$, 7 months. Data are representative of three independent immunoblots; eight eyes are from four mice. *B,* immunoblot detection of carbonyl-modified protein in ARPE-19 cells that accumulated A2E and were irradiated at 430 nm. *1st lane*, RPE; *2nd lane*, A2E-containing RPE; *3rd lane*, A2E-containing RPE irradiated with 430 nm light. Carbonyl content in total protein was analyzed by SDS-PAGE using a gradient gel and immunoblotting with anti-DNP antibody (*panel i*). *M* indicates molecular weight marker; +, carbonyl-BSA (positive control). The additional bands in the *3rd lane* and in the BSA lane (+) represent higher molecular weight derivatives related to adduct formation. Loading was controlled by re-probing with anti-β-actin antibody (42 kDa) (*panel ii*). Densitometric analysis (*panel iii*) of immunoreactive bands generated in two experiments. Carbonyl protein/actin ratios were normalized to untreated control and presented as mean ± S.E. *, $p < 0.05$ as compared with the other values; one-way ANOVA and Tukey's multiple comparison test. *C,* protein-carbonyl burden was measured by ELISA. ARPE-19 cells that had accumulated A2E were not irradiated (*A2E*) or irradiated (*A2E + 430 nm*) and then incubated for 2 or 6 h before the carbonyl was assayed. Mean ± S.E., three experiments. *, $p < 0.05$ as compared with A2E-containing cells that were not irradiated; one-way ANOVA and Newman-Keuls multiple comparisons test.

Detection of MG-Protein Adducts by ELISA—Of the biologically reactive dicarbonyls, MG is considered to be the most reactive (48). Because MG can form from intermediates of glycolysis (dihydroxyacetone phosphate and glyceraldehyde 3-phosphate) and in lesser quantities from fatty acid metabolism (3), we selected for MG generated by bisretinoid photodegradation by exposing mice (age 6 months) to in-cage 430 nm light for 2 h each day for a week (Fig. 2*A*). The content of MG-H1, an adduct of MG with arginine residues, was determined by indirect competitive ELISA using plates preabsorbed with MG conjugate and probed with antibody to MG-H1. The BSA equivalent concentrations were interpolated from standard curves generated by four-parameter analysis; the goodness of fit ($R2$) of the curve across three experiments ranged from 0.992 to 0.998. In both the $Abca4^{-/-}$ and $Rdh8^{-/-}/Abca4^{-/-}$ mutant mice, bisretinoid lipofuscin fluorophores accumulate at accelerated levels (27, 43, 44, 49). Accordingly, MG-BSA equiv-

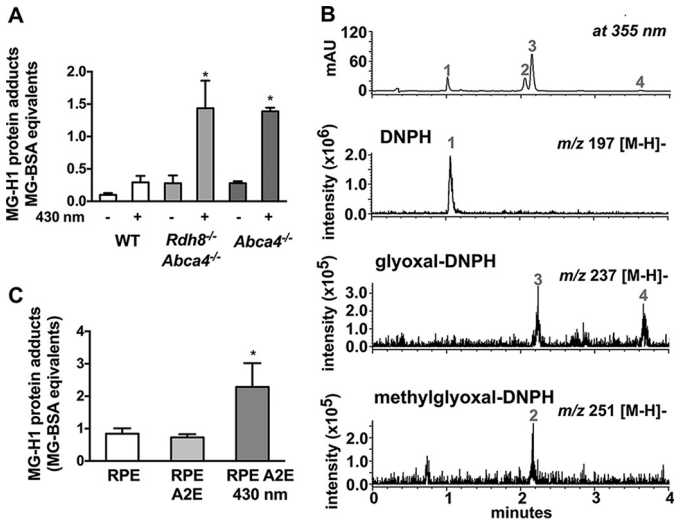

FIGURE 2. **Detection of MG adducts.** *A,* MG-derived hydroimidazolone protein adducts (MG-H1) in posterior eyecups of *Abca4*$^{+/+}$ wild type (WT), *Rdh8*$^{-/-}$/*Abca4*$^{-/-}$, and *Abca4*$^{-/-}$ mice (age 6 months) measured by competitive indirect ELISA. Mice were exposed (+) or not exposed (−) to blue light (430 nm) as a test of specificity. Detection using anti-MG antibody with MG-H1 quantification by interpolation from an MG-BSA standard curve (MG-BSA equivalents). Mean ± S.E., three experiments; four mice/eight eyes per group. *, $p < 0.05$ as compared with unexposed groups and wild-type 430 nm-exposed mice; one-way ANOVA and Tukey's multiple comparison test. *B,* UPLC-MS detection of DNPH-derivatized photocleavage products of A2E released upon irradiation (430 nm) of an A2E sample. Absorbance monitoring at 355 nm detects DNPH (*trace 1*), methylglyoxal-DNPH (*trace 2*), and glyoxal-DNPH (*trace 3*). MS-selected ion monitoring chromatograms at *m/z* 197 (DNPH) (*trace 1*), *m/z* 251 (methylglyoxal-DNPH) (*trace 2*), *m/z* 237 (glyoxal-DNPH) (*trace 3*), and an isomer of glyoxal-DNPH (*trace 4*). Data are representative of two experiments. *C,* measurement of MG-H1 protein adducts in lysates prepared from ARPE-19 cells that had accumulated A2E and were irradiated at 430 nm (*RPE A2E 430 nm*). Controls were RPE only and A2E-containing unirradiated RPE (*RPE A2E*). Mean ± S.E., three experiments. *, $p < 0.05$ as compared with other values; one-way ANOVA and Tukey's multiple comparison test.

alent levels were ~3-fold greater in *Abca4*$^{-/-}$ and *Rdh8*$^{-/-}$/*Abca4*$^{-/-}$ mice as compared with wild type; these MG-H1 levels are attributable at least in part, to the effects of ambient light during housing. Exposure of the mice to 430 nm light increased MG levels in all groups of mice; with pre-exposure to light, MG-BSA equivalent levels were almost 5-fold greater in the *Abca4*$^{-/-}$ and *Rdh8*$^{-/-}$/*Abca4*$^{-/-}$ mice as compared with wild-type *Abca4*$^{+/+}$ mice ($p < 0.05$). Intra-day and inter-day repeatability of the competitive ELISA was calculated using OD measures obtained for MG-BSA and was found to be 1.4 and 0.4%, respectively.

To corroborate our findings in mice, we also employed ARPE-19 cells that had accumulated a single bisretinoid, A2E (Fig. 2*C*). After we irradiated the A2E-containing ARPE-19 cells at 430 nm, we added the protein samples to 96-well ELISA plates preabsorbed with MG conjugate and probed with antibody to MG-H1. MG-BSA equivalent concentrations computed by four-parameter analysis were more than 4-fold higher in irradiated A2E-containing ARPE-19 cells as compared with non-irradiated companion cultures (Fig. 2*C*).

Detection of MG- and GO-DNPH by UPLC-MS—To demonstrate that MG and GO are released by photooxidation-associated photodegradation of the bisretinoid A2E, we also trapped these dicarbonyls by DNPH in cell-free experiments and analyzed by UPLC-MS. As shown in Fig. 2*B*, reaction of DNPH with 430 nm irradiated A2E yielded absorbances at 355 nm and the expected molecular ion products at *m/z* 237 and *m/z* 251 corresponding to glyoxal-DNPH and methylglyoxal-DNPH, respectively. The second *m/z* 237 peak is an isomer of glyoxal-DNPH. These results indicated that MG and GO are components of A2E photodegradation products.

Immunochemical Detection of Carbonylated Proteins in Mouse Eyes—Carbonylated proteins in sections of mouse eyes were visualized by derivatization with DNPH followed by detection using anti-DNP antibodies. As shown in Fig. 3, immunolabeling of DNPH-treated retina sections varied with the genotype and age of the mice. In *Abca4*$^{-/-}$ mice at 1 year of age, a dark line of immunostaining was readily visible on the basal side of the RPE monolayer in a location corresponding to Bruch's membrane (Fig. 3, *single-headed arrows*). In the retinas of *Abca4*$^{-/-}$ mice stained with rabbit polyclonal anti-MG antibody, a brown immunoreactive line was also observed basal to the RPE. Labeling here was less pronounced in wild-type *Abca4*$^{+/+}$ mice at 1 year and was not detected in 1-month-old mice. Diffuse brown immunoreactivity was also present in choroid but was less pronounced in sclera. The choroscleral interface is also prominent in these sections probably due to the combined effects of immunolabeling, uptake of hematoxylin, and refracting properties of this boundary.

Reaction of the polyclonal anti-MG antibody with adducts formed by photodegradation products of A2E was demonstrated by irradiating dot-blotted BSA in the presence of A2E (Fig. 3*B*, *panel b*). Commercial MG-BSA also reacted with the antibody (Fig. 3*B*, *panel c*) but unirradiated dot-blotted A2E and BSA were unreactive (Fig. 3*B*, *panel a*). The reactivity of the polyclonal anti-MG antibody was further corroborated by demonstrating similar reactivity with a mouse monoclonal anti-MG antibody (Fig. 3*B*, *panels e* and *f*).

AGE Deposition on Extracellular Collagen Substrate—The unhydrated forms of MG are hydrophobic and thus can pass through membranes (50, 51). In addition, extracellular deposition of MG and GO adducts contributes to tissue damage with the modified proteins having relatively long lifetimes (52). Thus, to determine whether the photooxidation/photodegradation of bisretinoid in RPE cells can result in the deposition of carbonyls on extracellular proteins, A2E-containing cultured RPE cells that had been grown on a substrate of collagen IV were irradiated at 430 nm (1.5 milliwatts/cm^2, 20 min), and after a 6-h incubation, the collagen was harvested. As shown in Fig. 4, rabbit polyclonal antibody to MG adducts reacted with immunoblotted collagen that had served as a substrate for the 430 nm irradiated A2E-containing RPE (*lane 3*). Immunoreactive bands were also detected when collagen was exposed to MG standard (Fig. 4, *lane 4*), but not when collagen was associated with A2E-free RPE or associated with non-irradiated A2E-containing RPE (Fig. 4, *lanes 1* and *2*).

Cross-linking of RNase A Protein by Products of Bisretinoid Photodegradation—The dicarbonyls methylglyoxal and glyoxal are known to react with side chains of lysine and arginine, and most studies indicate that cross-linking by dicarbonyls can involve both of these amino acid residues (53, 54). To determine whether carbonyls such MG and GO, when released upon pho-

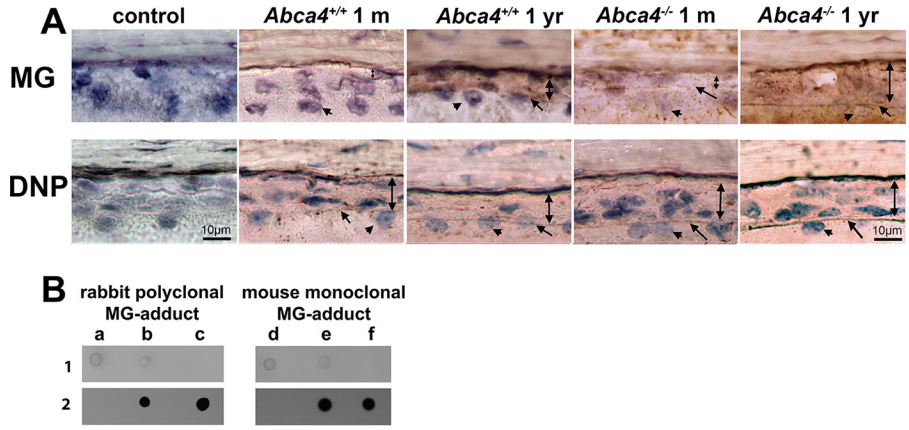

FIGURE 3. **Immunohistochemical labeling of methylglyoxal adducts and carbonyl adducts (DNP) in murine outer retina.** *A*, labeling with antibodies that recognize MG-derived hydroimidazolone protein adducts (MG-H1) (MG) and antibodies that recognize carbonyl groups derivatized with DNPH. Mutant mice and ages are indicated. *Control*, unreacted section. *Two-headed arrow*, choroid; *arrowhead,* RPE nuclei; *single-headed arrows*, Bruch's membrane. Data are representative of three experiments. The *dark line* on the basal side of RPE is indicative of Bruch's membrane staining. The interface between choroid and sclera is also visible. *B,* immunodot blot detection of MG adducts. Nitrocellulose membrane was visualized under white light (Nikon DSLR camera) immediately after samples were applied to the membrane (*row 1*) and by exposure to x-ray film following immune reaction (*row 2*). Blotted samples were A2E incubated with BSA (*a* and *d*) and A2E and BSA irradiated at 430 nm (*b* and *e*); commercial MG-BSA was positive control (*c* and *f*). Blotted samples (one experiment) were reacted with rabbit polyclonal anti-MG adduct (*a–c*) and mouse monoclonal anti-MG adducts (*d–f*) followed by HRP-conjugated secondary antibody and a luminol-based chemiluminescent substrate.

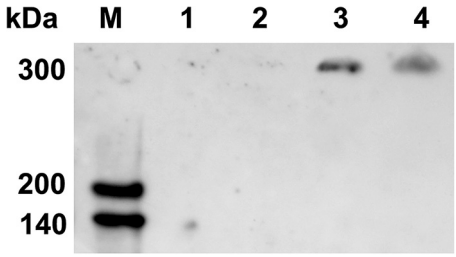

FIGURE 4. **Collagen (human type IV) serving as substrate for A2E-containing ARPE-19 cells is modified by MG after 430 nm irradiation.** Detection by Western blotting with rabbit polyclonal antibody to MG adducts. Cells grown on collagen substrate (*lane 1*), ARPE-19 cells on collagen substrate accumulated A2E (*lane 2*), A2E-containing RPE cells grown on collagen and irradiated at 430 nm for 20 min (*lane 3*), and collagen exposed to MG (positive control) (*lane 4*). Data are representative of three experiments.

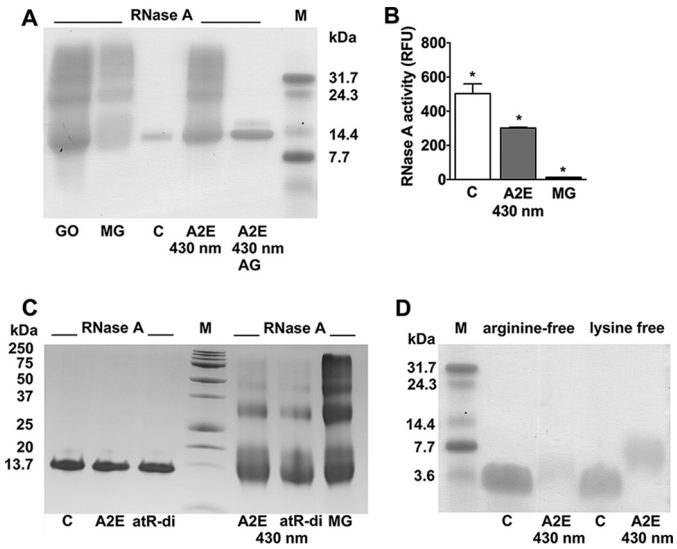

FIGURE 5. **Protein cross-linking by exposure to photodegradation products of all-*trans*-retinal dimer and A2E.** These photo-products are known to include MG and GO. *A,* RNase A (~14 kDa) as model protein was incubated (5 days; 37 °C) with A2E photodegraded by light irradiation at 430 nm (*A2E 430 nm*). Analysis was by SDS-PAGE. *GO*, MG-positive controls; *C*, RNase only control; *AG*, aminoguanidine. *M*, molecular mass markers. Data are representative of three experiments. *B,* RNase activity assay performed in absence (*C*, control) or presence of A2E that had been irradiated at 430 nm (*A2E 430 nm*) or MG, positive control. Mean ± S.E., four replicates; *, $p < 0.05$ as compared with control; one-way ANOVA, Newman-Keuls multiple comparison test. *C,* RNase A was incubated (5 days; 37 °C) with A2E or all-*trans*-retinal dimer (*atR-di*) (*left*) or with A2E photodegraded by light irradiation at 430 nm (*A2E 430 nm*) or with all-*trans*-retinal dimer photodegraded (*atR-di 430 nm*). *C*, RNase-only control; *MG*, positive control. Data are representative of three experiments. *D,* arginine-free (somatostatin) and lysine-free (renin) peptides. Conditions as in *A*. Dimers and smearing are indicative of higher molecular weight oligomers. *M*, molecular mass markers; *C* control. Data are representative of three experiments.

todegradation of A2E and all-*trans*-retinal dimer, can cross-link protein, we exposed RNase A (13.7 kDa) (5 days; 37 °C) to these 430 nm irradiated bisretinoids, and we analyzed by SDS-PAGE (Fig. 5*A*). RNase A contains both lysine and arginine (13.7 kDa, 10 lysine and 4 arginine residues) and is a good model for cross-linking studies because its small size enables detection of oligomeric forms (40, 55). Cross-linking after exposure to photodegraded A2E (Fig. 5*A*) was evidenced by SDS-PAGE with Coomassie Blue staining; RNase A dimers (~28 kDa) and higher oligomers ($n \times 14$ kDa) (56) were detected. Inclusion of the dicarbonyl scavenger aminoguanidine, which traps dicarbonyls before they can react with protein, protected against cross-linking, although in samples of RNase A incubated with commercially obtained MG and GO (positive control), higher molecular weight bands were prominent. An RNase A activity assay also showed that enzyme function was diminished by exposure of RNase A to photodegraded A2E (Fig. 5*B*). Similar findings were observed with exposure of RNase A to irradiated all-*trans*-retinal dimer and A2E in tandem (Fig. 5*C*). Here again, the presence of dimers and smearing were indicative of higher molecular weight oligomers.

Cross-linking by Photodegradation Products of A2E Was Observed with Both Lysine-free and Arginine-free Peptides—To further understand the structural correlates that enable cross-linking by photodegradation products of bisretinoid compounds such as A2E and all-*trans*-retinal dimer, we utilized

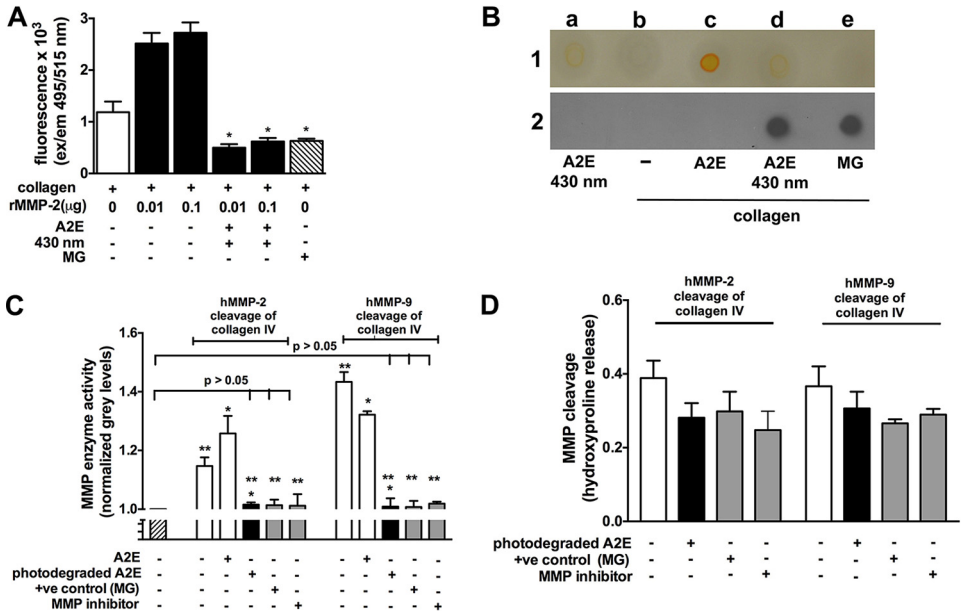

FIGURE 6. **Reduction in MMP-2 and MMP-9 activity induced by products of A2E photodegradation.** *A,* MMP-2 digestion of fluorescein-conjugated collagen IV is reduced after collagen is modified by dicarbonyls released by A2E photodegradation. Collagen and A2E mixture were irradiated at 430 nm and incubated with human recombinant MMP-2 (*rMMP-2*) at indicated concentration. *MG*, methylglyoxal (positive control). Fluorescence intensity (excitation/emission, 495/515 nm) is indicative of MMP-2 activity. Mean ± S.E., four replicates. *, significantly different from rMMP-2 digestion in absence of A2E/430 nm irradiation or MG; one-way ANOVA and Tukey's multiple comparison test. The value for MG treatment and the value for A2E/430 nm/0.1 μg of rMMP-2 treatment are not significantly different from untreated fluorescein-conjugated collagen. *B,* human collagen IV exposed to photodegradation products of A2E is modified by MG adducts. Immuno-dot blot detection. Nitrocellulose membrane was visualized under white light (Nikon DSLR camera) immediately after samples were applied to the membrane (*row 1*) and by exposure to x-ray film following immune reaction (*row 2*). All blotted samples (one experiment) were reacted with a rabbit polyclonal antibody that recognizes MG-modified protein, followed by HRP-conjugated secondary antibody, and a luminol-based chemiluminescent substrate. *Lane a,* A2E irradiated at 430 nm and then blotted in the absence of collagen; *lane b,* collagen in the absence of A2E; *lane c,* collagen incubated with non-irradiated A2E; *lane d,* collagen incubated at 37 °C with irradiated A2E; *lane e,* collagen incubated with methylglyoxal as positive control. *C*, zymography assay. Modification of collagen IV under conditions of A2E photodegradation reduces MMP-2 and MMP-9 cleavage of collagen IV. hMMP-2 and hMMP-9 activity was measured by densitometric analysis as described under "Experimental Procedures," and normalized ($GL_{MMP\ band} \div GL_{MMP\text{-}free}$) gray level intensities in the MMP lysis bands are presented. *Cross-hatched bar*, $GL_{MMP\text{-}free}$. Mean ± S.E. of three experiments; * $p < 0.05$, one-way ANOVA and Newman-Keuls multiple comparison test. *D*, MMP-2- and MMP-9-mediated cleavage was assayed by measuring the hydroxyproline content remaining in the zymography bands after MMP digestion. A decrease in hydroxyproline release from MMP bands is indicative of increased cross-linking of collagen and thus reduced MMP activity. Mean ± S.E. of two experiments.

defined peptides. Specifically, we reacted photodegraded A2E with somatostatin (AGCKNFFWKTFTSC; 14 residues) and a renin substrate tetradecapeptide (DRVYIHPFHLLVYS; 14 residues), two commercially available peptides that lack arginine and lysine, respectively (Fig. 5*D*). For the renin substrate, we used an *N*-protected form of the peptide to establish whether the presence of arginine alone (not the N terminus) was sufficient to permit reactivity. After a 5-day incubation of photooxidized/photodegraded A2E with the arginine-free peptide (somatostatin) that contains two lysine residues, a higher molecule weight band was visible that was not present in the control lane (Fig. 5*D*). With the lysine-free (renin substrate) peptide that contains one arginine, the unmodified peptide band was no longer visible, and a band of slightly higher molecular weight than the control peptide was observed (Fig. 5*D*). This band was not present in the control lane. The cross-linking of RNase A (Fig. 5*A*) appeared to be more pronounced than that of somatostatin and retinin substrate (Fig. 5*D*) even under the same concentration and conditions. This observation suggested that perhaps the majority of cross-links formed contain both lysine and arginine.

Modification of Collagen IV by Products of A2E Photodegradation Results in Reduced Cleavage by MMP2 and MMP9—Bruch's membrane undergoes continual remodeling by MMPs. MMP1–3 and -9 are secreted by RPE, and these MMPS are present in Bruch's membrane (57–59). Thus, we have also examined the ability of MMPs to act on collagen that had been exposed to photodegradation products of RPE bisretinoid. To this end, we tested human rMMP-2 activity on fluorescein-labeled collagen substrate (Molecular Probes, Life Technologies, Inc.) using an assay in which MMP-2 digestion is measured as an increase in fluorescence (excitation/emission 490/520 nm). MMP-2 digestion was reduced when the substrate had been exposed to A2E photodegradation products that included GO and MG (Fig. 6*A*) and with MG-positive control (Fig. 6*A*).

MG modification of the collagen IV substrate was confirmed on dot blots reacted with antibody that recognizes MG adducts (Fig. 6*B*). The orange coloration attributable to A2E when blotted together with collagen was readily visible (Fig. 6*B, row 1*, *panel c*). After irradiation, the orange chromophore disappeared due to photooxidation and degradation of A2E (Fig. 6*B*, *row 1*, *panel d*), although at the same location on the blot, collagen exhibited reactivity with the antibody to MG adducts (Fig. 6*B*, *row 2*, *panel d*). The collagen was also immunoreactive when MG standard was applied (Fig. 6*B*, *row 2*, *panel e*).

Modified Zymography—We next examined whether non-enzymatic reaction of collagen with A2E photodegradation products (including GO and MG) released by A2E irradiation (430 nm) interferes with collagen remodeling by MMPs *in vitro*. Here, hMMP-2 and hMMP-9 protein were added to the SDS-

polyacrylamide gel containing human collagen IV. By zymography, collagen IV inside the polyacrylamide gel was visualized by Coomassie Blue staining. Thus, in contrast to the darkly stained background of the gel, clear bands represented areas of MMP digestion by hMMP-2 and hMMP-9, with the position of the bands corresponding to the molecular weights of the MMP enzymes. We measured the gray level intensities of the MMP bands as an indication of MMP activity (Fig. 6*C*). As shown in Fig. 6*C*, pretreatment of collagen IV with photooxidized A2E greatly reduced grayscale intensities of the gel at the molecular weight positions corresponding to MMP-2 and MMP-9, indicating reduced MMP activity. A similar decrease in gray level was observed when the collagen was modified by incubation with MG and when an MMP inhibitor was employed (positive controls).

As an additional approach to quantifying the zymograms, we measured the collagen content of the MMP bands using hydroxyproline as a surrogate (Fig. 6*D*) (60). Hydroxyproline (4-hydroxyproline) is a hydroxylated form of proline that forms post-translationally, and in mammals it occurs only in collagen and elastin; hydroxyproline constitutes 14.4% of the amino acid composition of collagen in most mammalian tissues. To measure collagenolytic activity by assaying hydroxyproline, we measured the hydroxyproline remaining in the MMP bands at the molecular weight positions of the MMP-2 and MMP-9 bands and after subtraction plotted hydroxyproline released from the collagen at the molecular weight positions of MMP-2 and MMP-9. The hydroxyproline released from the MMP band obtained from untreated collagen exhibited the highest value; this would be expected due to the unrestricted release of hydroxyproline-containing collagen fragments during MMP digestion. When collagen was pretreated with MG (positive control) and photo-A2E, lower levels of hydroxyproline were released from the MMP-2- and MMP-9-associated collagen bands. The latter finding reflected a greater resistance to MMP-2- and MMP-9-mediated collagen cleavage. As expected, the liberation of hydroxyproline was also reduced when an MMP inhibitor was added.

RAGE RT-qPCR in Cells and Null Mutant Mice—The formation of carbonyl-modified protein is known to be paralleled by the regulated expression of the multiligand cell surface receptor RAGE (23). RAGE is expressed by numerous cell types, including intact RPE *in vivo* (19) and the cells of the ARPE-19 cell line (34). Moreover, it has been shown previously that RAGE expression increases in the presence of ligand (4, 18). RAGE expression was quantified by RT-qPCR in posterior eyecups of wild-type and mutant mice that varied in the levels of bisretinoid accumulation. Applying the comparative *Ct* method with the wild-type 4-month value assigned as comparator, we found that RAGE expression was greater in 6-month-old $Abca4^{-/-}$ mice than in 6-month-old $Abca4^{+/+}$ mice ($p < 0.05$) (Fig. 7*A*). Exposure of 6-month-old $Abca4^{-/-}$ and $Rdh8^{-/-}/Abca4^{-/-}$ mice to 430 nm light was also associated with a greater fold increase in RAGE expression relative to mice that were unexposed. In support of a link to bisretinoid levels, we also found that 430 nm exposure of ARPE-19 cells that had accumulated A2E was associated with a 2.5-fold increase in RAGE expression ($p < 0.05$) (Fig. 7*B*).

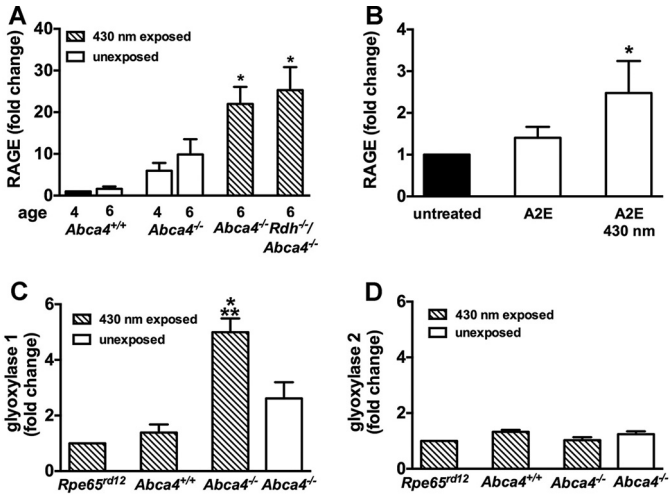

FIGURE 7. **RAGE, glyoxylase-1, and glyoxylase-2 expression.** RT-qPCR was performed with RNA purified from posterior eyecups of mice. *A,* RAGE expression was examined in $Abca4^{+/+}$ wild-type, $Abca4^{-/-}$, $Rdh8^{-/-}/Abca4^{-/-}$ mice, and $Rpe65^{rd12}$ mice at the ages indicated. The expression of each gene was normalized to 18S, and fold change in expression is presented relative to WT 4 months; three experiments. *B,* RAGE expression in ARPE-19 cells that had accumulated A2E and were irradiated at 430 nm (*A2E 430 nm*). Controls were untreated cells only and A2E-containing unirradiated RPE (*A2E*). Mean ± S.E., three experiments. *, $p < 0.05$ as compared with other values; one-way ANOVA and Dunnett's multiple comparison test. *C,* glyoxylase-1 expression was examined in $Rpe65^{rd12}$ (8 months), $Abca4^{+/+}$ (10 months), $Abca4^{-/-}$ 430 nm exposed (7 months), and $Abca4^{-/-}$ unexposed (11 months) mice and expressed relative to $Rpe65^{rd12}$. *, $p < 0.05$, as compared with $Rpe65^{rd12}$; **, $p < 0.05$ as compared with $Abca4^{+/+}$; one-way ANOVA and Tukey's multiple comparison test; two experiments. *D,* glyoxylase-2 expression was examined as in *C*. Mean ± S.E.; three experiments.

MG and GO are substrates for cytosolic glyoxylase 1, an enzyme that works with glutathione (GSH) to convert MG- and GO to D-lactate. Since upon their release MG and GO can induce glyoxylase 1 transcript levels (61, 62), we measured glyoxylase 1 mRNA by RT-qPCR (Fig. 7*C*). Here, we found that glyoxylase 1 mRNA was up-regulated in $Abca4^{-/-}$ mice exposed to 430 nm light, using $Rpe65^{rd12}$ sample as comparator. No change in glyoxylase 2 was observed (Fig. 7*D*).

Discussion

The end products of photodegradation of lipofuscin bisretinoids are a variety of reactive aldehydes and 3-carbon bifunctional fragments carrying two aldehydes (GO) or an aldehyde and a ketone (MG) (7, 8). The configuration of these fragments is consistent with the known polyene structures of bisretinoids (63). Non-enzymatic reactions between these electrophilic oxo-aldehydes and proteins constitute major forms of pathological post-translational modification and were originally identified as a class of AGEs (2). In this study, we probed for evidence that MG and GO can originate from bisretinoid constituents in RPE cells, hitherto an atypical source. We captured MG-arginine conjugates (MG-H1) in posterior eyecups of $Abca4^{-/-}$ and $Rdh8^{-/-}/Abca4^{-/-}$ mutant mice using a quantitative ELISA. The likelihood that the dicarbonyl-MG was generated from RPE bisretinoid lipofuscin was shown by demonstrating that the levels increased in mice harboring increased bisretinoid and in mice that were pre-exposed to 430 nm light. *In vivo* carbonylation specific to RPE cells in $Abca4^{-/-}$ mice was also shown by analysis of the RPE-specific protein Rpe65 in

immunoblots; carbonylation of Rpe65 likely reflects more generalized adduct formation in RPE cells. Additionally, in a cell model of bisretinoid photodegradation, protein carbonylation was demonstrated by ELISA and by Western blotting after carbonyl derivatization with DNPH, although MG-H1 was detected in the irradiated A2E-containing cells by ELISA with employment of antibody to MG-H1.

Abca4$^{-/-}$ mice are not only burdened with increased A2E (27, 43), photoreceptor cell loss is readily detectable in albino *Abca4*$^{-/-}$ mice (24, 25), and the retina is more susceptible to light damage (47). *Abca4*$^{-/-}$ mice also exhibit increased expression of proteins of the complement system, excessive complement activation, down-regulation of complement inhibitory proteins, and Bruch's membrane thickening due to basal laminar deposits (64). Analogous abnormalities are associated with enhanced deposition of the lipofuscin fluorophores A2E and all-*trans*-retinal dimer in RPE of *Rdh8*$^{-/-}$/*Abca4*$^{-/-}$ mice (49, 65, 66). These findings indicate a link between RPE lipofuscin and Bruch's membrane changes.

Focally organized drusen and diffuse deposits form in Bruch's membrane with age, and when of sufficient size and confluence, these deposits can confer risk for development of AMD (67, 68). Proteins in Bruch's membrane and drusen also undergo an age-dependent increase in carbonyl modifications (14, 15), which include adducts, fluorogenic products, and cross-linking species. Thus, it is significant that we found that exposure of peptides to reactive photodegradation products of the bisretinoids A2E and all-*trans*-retinal dimer resulted in covalent modifications. This adduct formation was associated with intermolecular cross-links and with reduced protein function. Moreover, aminoguanidine, a pharmaceutical that is a well known to trap reactive dicarbonyl compounds, inhibited cross-linking. A2E photodegradation products cross-linked a peptide containing both lysine and arginine and peptides containing either arginine or lysine. Together with the *in vivo* evidence that RPE lipofuscin can serve as the source of dicarbonyl adduct formation, these results indicate that reactive products released by photooxidation/photodegradation of bisretinoid lipofuscin fluorophores such as A2E and all-*trans*-retinal dimer have the capacity to form cross-linking species. These results are also likely informative as to the molecular basis for age-related Bruch's membrane thickening.

Disturbances in extracellular matrix turnover are also considered to contribute to Bruch's membrane thickening (70–72), and carbonyl modification of the resident proteins is implicated in the reduced ability of MMPs to degrade (73, 74). MMPs are regulated at stages of transcription, proenzyme activation, and enzyme inhibition (tissue inhibitors of metalloproteinases) (75). MMP expression in RPE and Bruch's membrane increases with age and oxidative stress (59, 76). In this study, we observed that exposure of collagen IV to A2E photodegradation products that include aldehyde-bearing fragments and the oxoaldehydes MG and GO, MMP activity was suppressed. This effect was observed by modified MMP zymography and by decreased release of MMP-cleaved hydroxyproline-containing fragments. These findings are consistent with the concept that molecular cross-linking confers resistance to remodeling by MMPs. In addition, deposition of carbonyl adducts on an extracellular collagen substrate after irradiation of intracellular A2E was demonstrated by immunoblotting with a rabbit polyclonal antibody that recognizes MG adducts. The observation that MG was bound to this extracellular substrate supports existing contentions that MG can easily diffuse across the membrane and covalently modify proteins at a distance from their origin (2). The potential importance of MMP regulation in Bruch's membrane is highlighted by Sorsby fundus dystrophy (77) wherein the gene mutated encodes tissue inhibitor of metalloproteinase-3 (TIMP3), a protein that is secreted by RPE and deposited into Bruch's membrane where it regulates turnover of extracellular matrix proteins. A region on chromosome 22 near TIMP3 is also linked to AMD (78). The phenotypes of exudative AMD and Sorsby fundus dystrophy have similarities that include choroidal neovascularization, drusen-like deposits, and RPE atrophy (79).

Besides the changes in protein function conferred by MG modifications, MG adducts exert cellular effects by interacting with the cell surface receptor RAGE (80, 81). We observed that RAGE transcript levels were increased in 430 nm exposed *Abca4*$^{-/-}$ and *Rdh8*$^{-/-}$/*Abca4*$^{-/-}$ mutant mice. RAGE is a multiligand receptor and one of a heterogeneous group of receptors responsible for downstream signaling by endogenous triggers of an inflammatory response (82). RPE cells constitutively express RAGE, and the expression of RAGE is up-regulated in RPE overlying drusen and other types of sub-RPE deposits (19, 83). AGES are deposited on Bruch's membrane with age (14, 84) and can be detected in sub-RPE deposits (85).

Proteins that are damaged by MG and GO modifications are conjugated with ubiquitin moieties for recognition and are then degraded by the ubiquitin-proteasome pathway (86), the chief non-lysosomal proteolytic system in cells (87). We previously showed in a cellular assay that photooxidative processes initiated by A2E increased ubiquitin-conjugating activity and elevated the cellular content of endogenous ubiquitin conjugates by more than 3-fold (88). A corresponding inhibition of peptidase activity together with an increase in availability of substrate for ubiquination accounted for the accumulation of ubiquitin conjugates (88). Moreover, an association with inflammatory processes was evidenced by an overproduction of interleukin-8 (IL-8) and interleukin-6 (IL-6) that paralleled the impairment of the ubiquitin-proteasome pathway (89).

To protect against adverse effects of MG, cells utilize detoxifying systems, primarily the glutathione (GSH)-dependent glyoxalase system (2). The glyoxalase system consists of the enzymes glyoxalase-1 and glyoxalase-2 and is the principal detoxifying pathway by which MG and GO are detoxified into D-lactate and glycolate, respectively. In the case of MG, the first step in the detoxification process is its non-enzymatic reaction with reduced GSH to form a hemithioacetal that is converted to (*S*)-D-lactoylglutathione by glyoxalase-1 (3). Glyoxalase-2 then catalyzes the transformation of (*S*)-lactoylglutathione into D-lactate and returns GSH to its reduced form. Because the glyoxalase system depends upon the availability of GSH, and NADPH produced by the pentose phosphate pathway is essential for the recycling of GSH from its oxidized form (GSSG) via glutathione reductase (3), the pentose phosphate pathway is also linked to MG detoxification. Accordingly, the efficiency of

glyoxalase detoxification pathways can be compromised by insufficient access to GSH and competition for NADPH. Indeed, although GSH is recycled by glyoxalase-2, the slower activity of glyoxalase-2 leaves some intracellular GSH trapped in the form of (*S*)-D-lactoylglutathione. Thus, exposure to MG could cause transient GSH deficiency.

Glyoxalase-1 is under stress-responsive control by the transcription factor Nrf2 (nuclear factor-erythroid 2 p45 subunit-related factor 2) through an antioxidant response element located in exon 1 of the mammalian glyoxalase-1 gene (62). Given the importance of the glyoxalase system, it is not surprising that we observed an increase in glyoxalase-1 transcripts in *Abca4*$^{-/-}$ mice pretreated with 430 nm light. Based on findings from colorimetric assays and by analysis using UPLC-MS, we previously reported that GSH can chemically reduce and form adducts with photodegradation products of A2E and specifically with MG (35). In cellular assays, we also demonstrated that sulforaphane, a phytochemical that increases the cellular content of GSH, can protect against the cellular damage associated with photooxidation of A2E (69).

We have explored a novel source of the dicarbonyls responsible for covalent modification of proteins. This source takes origin from the photodegradation of RPE bisretinoid and likely explains the accumulation of AGEs in drusen deposits underlying RPE. We propose that unlike the case for AGE modifications in diabetes, AGEs in drusen originate from the MG and GO released from overlying RPE. Some ongoing clinical studies aim to develop treatments for AMD and ABCA4-related blindness based on limiting RPE bisretinoid lipofuscin formation (90). The demonstrated link between RPE lipofuscin and Bruch's membrane changes could raise the possibility that therapies such as these may have benefits extending beyond effects on RPE bisretinoid accumulation alone; additional benefits could include preservation of Bruch's membrane integrity and easing of drusen load in the aging eye. There also exists the possibility of therapeutic crossover to AMD from other disorders such as diabetes, *e.g.* dicarbonyl scavengers and AGE receptor blockers.

Author Contributions—J. Zhou performed and analyzed experiments in Figs. 1–7. K. U. performed and analyzed experiments in Fig. 2; J. Zhao performed and analyzed experiments in Figure 3; J. R. S. designed experiments, assisted in analysis, interpreted data, and wrote the paper. All authors reviewed the results and approved the final version of the manuscript.

References

1. Pageon, H., Zucchi, H., Dai, Z., Sell, D. R., Strauch, C. M., Monnier, V. M., and Asselineau, D. (2015) Biological effects induced by specific advanced glycation end products in the reconstructed skin model of aging. *BioResearch* **4.1,** 54–64
2. Rabbani, N., and Thornalley, P. J. (2015) Dicarbonyl stress in cell and tissue dysfunction contributing to ageing and disease. *Biochem. Biophys. Res. Commun.* **458,** 221–226
3. Allaman, I., Belanger, M., and Magistretti, P. J. (2015) Methylglyoxal, the dark side of glycolysis. *Frontiers Neurosci.* **9,** 1–12
4. Manigrasso, M. B., Juranek, J., Ramasamy, R., and Schmidt, A. M. (2014) Unlocking the biology of RAGE in diabetic microvascular complications. *Trends Endocrinol. Metab.* **25,** 15–22
5. Thornalley, P. J. (2008) Protein and nucleotide damage by glyoxal and methylglyoxal in physiological systems–role in ageing and disease. *Drug Metabol. Drug Interact.* **23,** 125–150
6. Wilker, S. C., Chellan, P., Arnold, B. M., and Nagaraj, R. H. (2001) Chromatographic quantification of argpyrimidine, a methylglyoxal-derived product in tissue proteins: comparison with pentosidine. *Anal. Biochem.* **290,** 353–358
7. Wu, Y., Yanase, E., Feng, X., Siegel, M. M., and Sparrow, J. R. (2010) Structural characterization of bisretinoid A2E photocleavage products and implications for age-related macular degeneration. *Proc. Natl. Acad. Sci. U.S.A.* **107,** 7275–7280
8. Yoon, K. D., Yamamoto, K., Ueda, K., Zhou, J., and Sparrow, J. R. (2012) A novel source of methylglyoxal and glyoxal in retina: implications for age-related macular degeneration. *PLoS One* **7,** e41309
9. Ramrattan, R. S., van der Schaft, T. L., Mooy, C. M., Bruijn, W. C., Mulder, P. G. H., and de Jong, P. T. V. M. (1994) Morphometric analysis of Bruch's membrane–the choriocapillaris and the choroid in aging. *Invest. Ophthalmol Vis. Sci.* **35,** 1857–2864
10. Curcio, C. A., Johnson, M., Huang, J.-D., and Rudolf, M. (2010) Apolipoprotein B-containing lipoproteins in retinal aging and age-related macular degeneration. *J. Lipid Res.* **51,** 451–467
11. Booij, J. C., Baas, D. C., Beisekeeva, J., Gorgels, T. G., and Bergen, A. A. (2010) The dynamic nature of Bruch's membrane. *Prog. Retin. Eye Res.* **29,** 1–18
12. Hussain, A. A., Starita, C., Hodgetts, A., and Marshall, J. (2010) Macromolecular diffusion characteristics of ageing human Bruch's membrane: implications for age-related macular degeneration (AMD). *Exp. Eye Res.* **90,** 703–710
13. Hageman, G. S., and Mullins, R. F. (1999) Molecular composition of drusen as related to substructural phenotype. *Mol. Vis.* **5,** 28–37
14. Handa, J. T., Verzijl, N., Matsunaga, H., Aotaki-Keen, A., Lutty, G. A., te Koppele, J. M., Miyata, T., and Hjelmeland, L. M. (1999) Increase in advanced glycation end product pentosidine in Bruch's membrane with age. *Invest. Ophthalmol. Vis. Sci.* **40,** 775–779
15. Crabb, J. W., Miyagi, M., Gu, X., Shadrach, K., West, K. A., Sakaguchi, H., Kamei, M., Hasan, A., Yan, L., Rayborn, M. E., Salomon, R. G., and Hollyfield, J. G. (2002) Drusen proteome analysis: an approach to the etiology of age-related macular degeneration. *Proc. Natl. Acad. Sci. U.S.A.* **99,** 14682–14687
16. Ott, C., Jacobs, K., Haucke, E., Navarrete Santos, A., Grune, T., and Simm, A. (2014) Role of advanced glycation end products in cellular signaling. *Redox Biol.* **2,** 411–429
17. Tian, J., Ishibashi, K., Ishibashi, K., Reiser, K., Grebe, R., Biswal, S., Gehlbach, P., and Handa, J. T. (2005) Advanced glycation end product-induced aging of the retinal pigment epithelium and choroid: a comprehensive transcriptional response. *Proc. Natl. Acad. Sci. U.S.A.* **102,** 11846–11851
18. Yuan, X., Gu, X., Crabb, J. S., Yue, X., Shadrach, K., Hollyfield, J. G., and Crabb, J. W. (2010)) Quantitative proteomics: comparison of the macular Bruch's membrane/choroid complex from age-related macular degeneration and normal eyes. *Mol. Cell. Proteomics* **9,** 1031–1046
19. Yamada, Y., Ishibashi, K., Ishibashi, K., Bhutto, I. A., Tian, J., Lutty, G. A., and Handa, J. T. (2006) The expression of advanced glycation end product receptors in RPE cells associated with basal deposits in human maculas. *Exp. Eye Res.* **82,** 840–848
20. Cano, M., Fijalkowski, N., Kondo, N., Dike, S., and Handa, J. (2011) Advanced glycation end product changes to Bruch's membrane promotes lipoprotein retention by lipoprotein lipase. *Am. J. Pathol.* **179,** 850–859
21. Bondeva, T., Wojciech, S., and Wolf, G. (2011) Advanced glycation end products inhibit adhesion ability of differentiated podocytes in a neuropilin-1-dependent manner. *Am. J. Physiol. Renal Physiol* **301,** F852-F870
22. Schmidt, A. M., Hasu, M., Popov, D., Zhang, J. H., Chen, J., Yan, S. D., Brett, J., Cao, R., Kuwabara, K., and Costache, G. (1994) Receptor for advanced glycation end products (AGEs) has a central role in vessel wall interactions and gene activation in response to circulating AGE proteins. *Proc. Natl. Acad. Sci. U.S.A.* **91,** 8807–8811
23. Litwinoff, E., Hurtado Del Pozo, C., Ramasamy, R., and Schmidt, A. M.

(2015) Emerging targets for therapeutic development in diabetes and its complications: the RAGE signaling pathway. *Clin. Pharmacol. Ther.* **98,** 135–144
24. Radu, R. A., Yuan, Q., Hu, J., Peng, J. H., Lloyd, M., Nusinowitz, S., Bok, D., and Travis, G. H. (2008) Accelerated accumulation of lipofuscin pigments in the RPE of a mouse model for ABCA4-mediated retinal dystrophies following vitamin A supplementation. *Invest. Ophthalmol. Vis. Sci.* **49,** 3821–3829
25. Wu, L., Nagasaki, T., and Sparrow, J. R. (2010) Photoreceptor cell degeneration in $Abcr^{-/-}$ mice. *Adv. Exp. Med. Biol.* **664,** 533–539
26. Sparrow, J. R., Blonska, A., Flynn, E., Duncker, T., Greenberg, J. P., Secondi, R., Ueda, K., and Delori, F. C. (2013) Quantitative fundus autofluorescence in mice: correlation with HPLC quantitation of RPE lipofuscin and measurement of retina outer nuclear layer thickness. *Invest. Ophthalmol. Vis. Sci.* **54,** 2812–2820
27. Kim, S. R., Fishkin, N., Kong, J., Nakanishi, K., Allikmets, R., and Sparrow, J. R. (2004) The Rpe65 Leu450Met variant is associated with reduced levels of the RPE lipofuscin fluorophores A2E and iso-A2E. *Proc. Natl. Acad. Sci. U.S.A.* **101,** 11668–11672
28. Mattapallil, M. J., Wawrousek, E. F., Chan, C. C., Zhao, H., Roychoudhury, J., Ferguson, T. A., and Caspi, R. R. (2012) The Rd8 mutation of the Crb1 gene is present in vendor lines of C57BL/6N mice and embryonic stem cells, and confounds ocular induced mutant phenotypes. *Invest. Ophthalmol. Vis. Sci.* **53,** 2921–2927
29. Sparrow, J. R., Wu, Y., Nagasaki, T., Yoon, K. D., Yamamoto, K., and Zhou, J. (2010) Fundus autofluorescence and the bisretinoids of retina. *Photochem. Photobiol. Sci.* **9,** 1480–1489
30. Parish, C. A., Hashimoto, M., Nakanishi, K., Dillon, J., and Sparrow, J. (1998) Isolation and one-step preparation of A2E and iso-A2E, fluorophores from human retinal pigment epithelium. *Proc. Natl. Acad. Sci. U.S.A.* **95,** 14609–14613
31. Fishkin, N. E., Sparrow, J. R., Allikmets, R., and Nakanishi, K. (2005) Isolation and characterization of a retinal pigment epithelial cell fluorophore: an all-*trans*-retinal dimer conjugate. *Proc. Natl. Acad. Sci. U.S.A.* **102,** 7091–7096
32. Sparrow, J. R., Parish, C. A., Hashimoto, M., and Nakanishi, K. (1999) A2E, a lipofuscin fluorophore, in human retinal pigmented epithelial cells in culture. *Invest. Ophthalmol. Vis. Sci.* **40,** 2988–2995
33. Sparrow, J. R., Zhou, J., Ben-Shabat, S., Vollmer, H., Itagaki, Y., and Nakanishi, K. (2002) Involvement of oxidative mechanisms in blue light induced damage to A2E-laden RPE. *Invest. Ophthalmol. Vis. Sci.* **43,** 1222–1227
34. Zhou, J., Cai, B., Jang, Y. P., Pachydaki, S., Schmidt, A. M., and Sparrow, J. R. (2005) Mechanisms for the induction of HNE-MDA- and AGE-adducts, RAGE and VEGF in retinal pigment epithelial cells. *Exp. Eye Res.* **80,** 567–580
35. Yoon, K. D., Yamamoto, K., Zhou, J., and Sparrow, J. R. (2011) Photoproducts of retinal pigment epithelial bisretinoids react with cellular thiols. *Mol. Vis.* **17,** 1839–1849
36. Talent, J. M., Kong, Y., and Gracy, R. W. (1998) A double stain for total and oxidized proteins from two-dimensional fingerprints. *Anal. Biochem.* **263,** 31–38
37. Linares, M., Marin-Garcíía, P., Méndez, D., Puyet, A., Diez, A., and Bautista, J. M. (2011) Proteomic approaches to identifying carbonylated proteins in brain tissue. *J. Proteome Res.* **10,** 1719–1727
38. Canellas, P. F., and Karu, A. E. (1981) Statistical package for analysis of competition ELISA results. *J. Immunol. Methods* **47,** 375–385
39. Wu, Y., Fishkin, N. E., Pande, A., Pande, J., and Sparrow, J. R. (2009) Novel lipofuscin bisretinoids prominent in human retina and in a model of recessive Stargardt disease. *J. Biol. Chem.* **284,** 20155–20166
40. Meade, S. J., Miller, A. G., and Gerrard, J. A. (2003) The role of dicarbonyl compounds in non-enzymatic crosslinking: a structure-activity study. *Bioorg Med. Chem.* **11,** 853–862
41. Miller, A. G., Meade, S. J., and Gerrard, J. A. (2003) New insights into protein crosslinking via the Maillard reaction: structural requirements, the effect on enzyme function, and predicted efficacy of crosslinking inhibitors as anti-ageing therapeutics. *Bioorg Med. Chem.* **11,** 843–852
42. Schmittgen, T. D., and Livak, K. J. (2008) Analyzing real-time PCR data by the comparative $C(T)$ method. *Nat. Protoc.* **3,** 1101–1108
43. Weng, J., Mata, N. L., Azarian, S. M., Tzekov, R. T., Birch, D. G., and Travis, G. H. (1999) Insights into the function of Rim protein in photoreceptors and etiology of Stargardt's disease from the phenotype in abcr knockout mice. *Cell* **98,** 13–23
44. Kim, S. R., Jang, Y. P., Jockusch, S., Fishkin, N. E., Turro, N. J., and Sparrow, J. R. (2007) The all-*trans*-retinal dimer series of lipofuscin pigments in retinal pigment epithelial cells in a recessive Stargardt disease model. *Proc. Natl. Acad. Sci. U.S.A.* **104,** 19273–19278
45. Dalle-Donne, I., Rossi, R., Giustarini, D., Milzani, A., and Colombo, R. (2003) Protein carbonyl groups as biomarkers of oxidative stress. *Clin. Chim. Acta* **329,** 23–38
46. Pang, J. J., Chang, B., Hawes, N. L., Hurd, R. E., Davisson, M. T., Li, J., Noorwez, S. M., Malhotra, R., McDowell, J. H., Kaushal, S., Hauswirth, W. W., Nusinowitz, S., Thompson, D. A., and Heckenlively, J. R. (2005) Retinal degeneration 12 (rd12): a new, spontaneously arising mouse model for human Leber congenital amaurosis (LCA). *Mol. Vis.* **11,** 152–162
47. Wu, L., Ueda, K., Nagasaki, T., and Sparrow, J. R. (2014) Light damage in Abca4 and Rpe65rd12 mice. *Invest. Ophthalmol. Vis. Sci.* **55,** 1910–1918
48. Shinohara, M., Thornalley, P. J., Giardino, I., Beisswenger, P., Thorpe, S. R., Onorato, J., and Brownlee, M. (1998) Overexpression of glyoxalase-I in bovine endothelial cells inhibits intracellular advanced glycation end product formation and prevents hyperglycemia-induced increases in macromolecular endocytosis. *J. Clin. Invest.* **101,** 1142–1147
49. Maeda, A., Golczak, M., Maeda, T., and Palczewski, K. (2009) Limited roles of Rdh8, Rdh12, and Abca4 in all-*trans*-retinal clearance in mouse retina. *Invest. Ophthalmol. Vis. Sci.* **50,** 5435–5443
50. Rabbani, N., and Thornalley, P. J. (2014) Measurement of methylglyoxal by stable isotopic dilution analysis LC-MS/MS with corroborative prediction in physiological samples. *Nat. Protoc.* **9,** 1969–1979
51. Abordo, E. A., Minhas, H. S., and Thornalley, P. J. (1999) Accumulation of α-oxoaldehydes during oxidative stress: a role in cytotoxicity. *Biochem. Pharmacol.* **58,** 641–648
52. Voziyan, P., Brown, K. L., Chetyrkin, S., and Hudson, B. (2014) Site-specific AGE modifications in the extracellular matrix: a role for glyoxal in protein damage in diabetes. *Clin. Chem. Lab. Med.* **52,** 39–45
53. Odani, H., Shinzato, T., Usami, J., Matsumoto, Y., Brinkmann Frye, E., Baynes, J. W., and Maeda, K. (1998) Imidazolium crosslinks derived from reaction of lysine with glyoxal and methylglyoxal are increased in serum proteins of uremic patients: evidence for increased oxidative stress in uremia. *FEBS Lett.* **427,** 381–385
54. Chellan, P., and Nagaraj, R. H. (2001) Early glycation products produce pentosidine cross-links on native proteins. novel mechanism of pentosidine formation and propagation of glycation. *J. Biol. Chem.* **276,** 3895–3903
55. Raines, R. T. (1998) Ribonuclease A. *Chem. Rev.* **98,** 1045–1066
56. Simons, B. L., King, M. C., Cyr, T., Hefford, M. A., and Kaplan, H. (2002) Covalent cross-linking of proteins without chemical reagents. *Protein Sci.* **11,** 1558–1564
57. Alexander, J. P., Bradley, J. M., Gabourel, J. D., and Acott, T. S. (1990) Expression of matrix metalloproteinases and inhibitor by human retinal pigment epithelium. *Invest. Ophthalmol. Vis. Sci.* **31,** 2520–2528
58. Hunt, R. C., Fox, A., al Pakalnis, V., Sigel, M. M., Kosnosky, W., Choudhury, P., and Black, E. P. (1993) Cytokines cause cultured retinal pigment epithelial cells to secrete metalloproteinases and to contract collagen gels. *Invest. Ophthalmol. Vis. Sci.* **34,** 3179–3186
59. Guo, L., Hussain, A. A., Limb, G. A., and Marshall, J. (1999) Age-dependent variation in metalloproteinase activity of isolated human Bruch's membrane and choroid. *Invest. Ophthalmol. Vis. Sci.* **40,** 2676–2682
60. Sabeh, F., Ota, I., Holmbeck, K., Birkedal-Hansen, H., Soloway, P., Balbin, M., Lopez-Otin, C., Shapiro, S., Inada, M., Krane, S., Allen, E., Chung, D., and Weiss, S. J. (2004) Tumor cell traffic through the extracellular matrix is controlled by the membrane-anchored collagenase MT1-MMP. *J. Cell Biol.* **167,** 769–781
61. Kurz, A., Rabbani, N., Walter, M., Bonin, M., Thornalley, P., Auburger, G., and Gispert, S. (2011) α-Synuclein deficiency leads to increased glyoxalase 1 expression and glycation stress. *Cell Mol. Life Sci.* **68,** 721–733
62. Xue, M., Rabbani, N., Momiji, H., Imbasi, P., Anwar, M. M., Kitteringham,

N., Park, B. K., Souma, T., Moriguchi, T., Yamamoto, M., and Thornalley, P. J. (2012) Transcriptional control of glyoxalase 1 by Nrf2 provides a stress-responsive defence against dicarbonyl glycation. *Biochem. J.* **443,** 213–222

63. Sparrow, J. R., Gregory-Roberts, E., Yamamoto, K., Blonska, A., Ghosh, S. K., Ueda, K., and Zhou, J. (2012) The bisretinoids of retinal pigment epithelium. *Prog. Retin. Eye Res.* **31,** 121–135
64. Radu, R. A., Hu, J., Yuan, Q., Welch, D. L., Makshanoff, J., Lloyd, M., McMullen, S., Travis, G. H., and Bok, D. (2011) Complement system dysregulation and inflammation in the retinal pigment epithelium of a mouse model for Stargardt macular degeneration. *J. Biol. Chem.* **286,** 18593–18601
65. Maeda, A., Maeda, T., Golczak, M., and Palczewski, K. (2008) Retinopathy in mice induced by disrupted all-*trans*-retinal clearance. *J. Biol. Chem.* **283,** 26684–26693
66. Flynn, E., Ueda, K., Auran, E., Sullivan, J. M., and Sparrow, J. R. (2014) Fundus autofluorescence and photoreceptor cell rosettes in mouse models. *Invest. Ophthalmol. Vis. Sci.* **55,** 5643–5652
67. Davis, M. D., Gangnon, R. E., Lee, L. Y., Hubbard, L. D., Klein, B. E., Klein, R., Ferris, F. L., Bressler, S. B., Milton, R. C., and Age-Related Eye Disease Study Group (2005) The Age-Related Eye Disease Study severity scale for age-related macular degeneration: AREDS Report No. 17. *Arch. Ophthalmol.* **123,** 1484–1498
68. Pauleikhoff, D., Barondes, M. J., Minassian, D., Chisholm, I. H., and Bird, A. C. (1990) Drusen as risk factors in age-related macular disease. *Am. J. Ophthalmol.* **109,** 38–43
69. Zhou, J., Gao, X., Cai, B., and Sparrow, J. R. (2006) Indirect antioxidant protection against photooxidative processes initiated in retinal pigment epithelial cells by a lipofuscin pigment. *Rejuven. Res.* **9,** 256–263
70. Cousins, S. W., Marin-Castaño, M. E., Espinosa-Heidmann, D. G., Alexandridou, A., Striker, L., and Elliot, S. (2003) Female gender, estrogen loss, and sub-RPE deposit formation in aged mice. *Invest. Ophthalmol. Vis. Sci.* **44,** 1221–1229
71. Kumar, A., El-Osta, A., Hussain, A. A., and Marshall, J. (2010) Increased sequestration of matrix metalloproteinases in ageing human Bruch's membrane: implications for ECM turnover. *Invest. Ophthalmol. Vis. Sci.* **51,** 2664–2670
72. Hussain, A. A., Lee, Y., Zhang, J. J., and Marshall, J. (2011) Disturbed matrix metalloproteinase activity of Bruch's membrane in age-related macular degeneration. *Invest. Ophthalmol. Vis. Sci.* **52,** 4459–4466
73. Mott, J. D., Khalifah, R. G., Nagase, H., Shield, C. F. 3rd, Hudson, J. K., and Hudson, B. G. (1997) Nonenzymatic glycation of type IV collagen and matrix metalloproteinase susceptibility. *Kidney Int.* **52,** 1302–1312
74. Nagai, N., Klimava, A., Lee, W. H., Izumi-Nagai, K., and Handa, J. T. (2009) CTGF is increased in basal deposits and regulates matrix production through the ERK (p42/p44mapk) MAPK and the p38 MAPK signaling pathways. *Invest. Ophthalmol. Vis. Sci.* **50,** 1903–1910
75. Sivak, J. M., and Fini, M. E. (2002) MMPs in the eye: emerging roles for matrix metalloproteinases in ocular physiology. *Prog. Retin. Eye Res.* **21,** 1–14
76. Alge-Priglinger, C. S., Kreutzer, T., Obholzer, K., Wolf, A., Mempel, M., Kernt, M., Kampik, A., and Priglinger, S. G. (2009) Oxidative stress-mediated induction of MMP-1 and MMP-3 in human RPE cells. *Invest. Ophthalmol. Vis. Sci.* **50,** 5495–5503
77. Weber, B. H., Vogt, G., Pruett, R. C., Stöhr, H., and Felbor, U. (1994) Mutations in the tissue inhibitor of metalloproteinases-3 (TIMP3) in patients with Sorsby's fundus dystrophy. *Nat. Genet.* **8,** 352–356
78. Chen, W., Stambolian, D., Edwards, A. O., Branham, K. E., Othman, M., Jakobsdottir, J., Tosakulwong, N., Pericak-Vance, M. A., Campochiaro, P. A., Klein, M. L., Tan, P. L., Conley, Y. P., Kanda, A., Kopplin, L., Li, Y., Augustaitis, K. J., *et al.* (2010) Genetic variants near TIMP3 and high-density lipoprotein-associated loci influence susceptibility to age-related macular degeneration. *Proc. Natl. Acad. Sci. U.S.A.* **107,** 7401–7406
79. Gliem, M., Müller, P. L., Mangold, E., Holz, F. G., Bolz, H. J., Stöhr, H., Weber, B. H., and Charbel Issa, P. (2015) Sorsby Fundus Dystrophy: novel mutations, novel phenotypic characteristics, and treatment outcomes. *Invest. Ophthalmol. Vis. Sci.* **56,** 2664–2676
80. Grillo, M. A., and Colombatto, S. (2008) Advanced glycation end-products (AGEs): involvement in aging and in neurodegenerative diseases. *Amino Acids* **35,** 29–36
81. Schmidt, A. M. (2015) Soluble RAGEs–prospects for treating & tracking metabolic and inflammatory disease. *Vascul. Pharmacol.* **72,** 1–8
82. Schaefer, L. (2014) Complexity of danger: the diverse nature of damage-associated molecular patterns. *J. Biol. Chem.* **289,** 35237–35245
83. Howes, K. A., Liu, Y., Dunaief, J. L., Milam, A., Frederick, J. M., Marks, A., and Baehr, W. (2004) Receptor for advanced glycation end products and age-related macular degeneration. *Invest. Ophthalmol. Vis. Sci.* **45,** 3713–3720
84. Glenn, J. V., Mahaffy, H., Wu, K., Smith, G., Nagai, R., Simpson, D. A., Boulton, M. E., and Stitt, A. W. (2009) Advanced glycation end product (AGE) accumulation on Bruch's membrane: links to age-related RPE dysfunction. *Invest. Ophthalmol. Vis. Sci.* **50,** 441–451
85. Ishibashi, T., Murata, T., Hangai, M., Nagai, R., Horiuchi, S., Lopez, P. F., Hinton, D. R., and Ryan, S. J. (1998) Advanced glycation end products in age-related macular degeneration. *Arch. Ophthalmol.* **116,** 1629–1632
86. Bento, C. F., Fernandes, R., Ramalho, J., Marques, C., Shang, F., Taylor, A., and Pereira, P. (2010) The chaperone-dependent ubiquitin ligase CHIP targets HIF-1α for degradation in the presence of methylglyoxal. *PLoS ONE* **5,** e15062
87. Martens, S., and Bachmair, A. (2015) How cells coordinate waste removal through their major proteolytic pathways. *Nature Cell Biol.* **17,** 841–842
88. Zhang, X., Zhou, J., Fernandes, A. F., Sparrow, J. R., Pereira, P., Taylor, A., and Shang, F. (2008) The proteasome: a target of oxidative damage in cultured human retina pigment epithelial cells. *Invest. Ophthalmol. Vis. Sci.* **49,** 3622–3630
89. Fernandes, A. F., Zhou, J., Zhang, X., Bian, Q., Sparrow, J., Taylor, A., Pereira, P., and Shang, F. (2008) Oxidative inactivation of the proteasome in retinal pigment epithelial cells. A potential link between oxidative stress and up-regulation of interleukin-8. *J. Biol. Chem.* **283,** 20745–20753
90. Zarbin, M. A., and Rosenfeld, P. J. (2010) Pathway-based therapies for age-related macular degeneration. An integrated survey of emerging treatment alternatives. *Retina* **30,** 1350–1367